PAPER

Polypeptide vesicles with densely packed multilayer membranes†

Ziyuan Song,‡[a] Hojun Kim,‡[a] Xiaochu Ba,[b] Ryan Baumgartner,[b] Jung Seok Lee,[a] Haoyu Tang,[a] Cecilia Leal*[a] and Jianjun Cheng*[ab]

Multilamellar membranes are important building blocks for constructing self-assembled structures with improved barrier properties, such as multilamellar lipid vesicles. Polymeric vesicles (polymersomes) have attracted growing interest, but multilamellar polymersomes are much less explored. Here, we report the formation of polypeptide vesicles with unprecedented densely packed multilayer membrane structures with poly(ethylene glycol)-*block*-poly(γ-(4,5-dimethoxy-2-nitrobenzyl)-ʟ-glutamate) (PEG-*b*-PL), an amphiphilic diblock rod-coil copolymer containing a short PEG block and a short hydrophobic rod-like polypeptide segment. The polypeptide rods undergo smectic ordering with PEG buried between the hydrophobic polypeptide layers. The size of both blocks and the rigidity of the hydrophobic polypeptide block are critical in determining the membrane structures. Increase of the PEG length in PEG-*b*-PL results in the formation of bilayer sheets, while using random-coil polypeptide block leads to the formation of large compound micelles. UV treatment causes ester bond cleavage of the polypeptide side chain, which induces helix-to-coil transition, change of copolymer amphiphilicity, and eventual disassembly of vesicles. These polypeptide vesicles with unique membrane structures provide a new insight into self-assembly structure control by precisely tuning the composition and conformation of polymeric amphiphiles.

Introduction

Polymeric vesicles (or polymersomes) have found broad applications in encapsulation and drug delivery.[1–7] Amphiphilic block copolymers with coil–coil structures are often used to form sandwich-like 2D curved membrane structures with a hydrophobic wall and hydrophilic inner and outer coronas.[1,2] A hydrophobic polymer segment with high molecular weight (MW) is essential to ensure strong interactions between chains (*e.g.*, chain entanglement and/or hydrophobic interaction) to form a kinetically frozen hydrophobic layer with appropriate toughness.[8] In addition, the strong interactions are necessary to impart low membrane permeability for the stable encapsulation of cargo.[1,9] Although polymersomes are structurally related to liposomes, as both are vesicles with hollow interiors, one key structural difference is that liposomes have well packed short lipid bilayer structures whereas polymersomes are based on randomly entangled long hydrophobic polymers. Control over the stability and membrane permeability of polymersomes rather than the detailed molecular arrangement in the hydrophobic layer has been largely the focus of study in the past 20 years.[1,2,9–11]

In contrast to coil–coil block copolymers, rod-coil block copolymers have received increasing attention in solution self-assembly due to the special rigid conformation of the rod blocks.[12–14] The anisotropic alignment of hydrophobic rods favors the formation of 2D membranes with lower curvature rather than the formation of spherical micelles.[2,14] Polypeptides, a class of polymeric biomaterials with broad biological and biomedical applications,[15–21] can adopt rigid α-helical conformation and have been demonstrated to be excellent rod-like building blocks for vesicle membranes.[22–24] For instance, Deming *et al.* first reported polypeptide vesicles through the conformation-specific self-assembly of amphiphilic diblock copolypeptides.[25,26] Membrane stability was enhanced by the preferred side-by-side alignment of rigid rod-like hydrophobic polypeptide helices along the helical axis and the lower conformational entropy loss during the assembly process.[2,9] The detailed polypeptide vesicle membrane structures, however, have never been fully studied, although they are believed to form very thin hydrophobic layers (several nanometers) with the suggested unilamellar membrane

[a] Department of Materials Science and Engineering, University of Illinois at Urbana–Champaign, 1304 West Green Street, Urbana, Illinois 61801, USA. E-mail: jianjunc@illinois.edu

[b] Department of Chemistry, University of Illinois at Urbana–Champaign, 505 South Mathews Avenue, Urbana, Illinois 61801, USA. E-mail: cecilial@illinois.edu
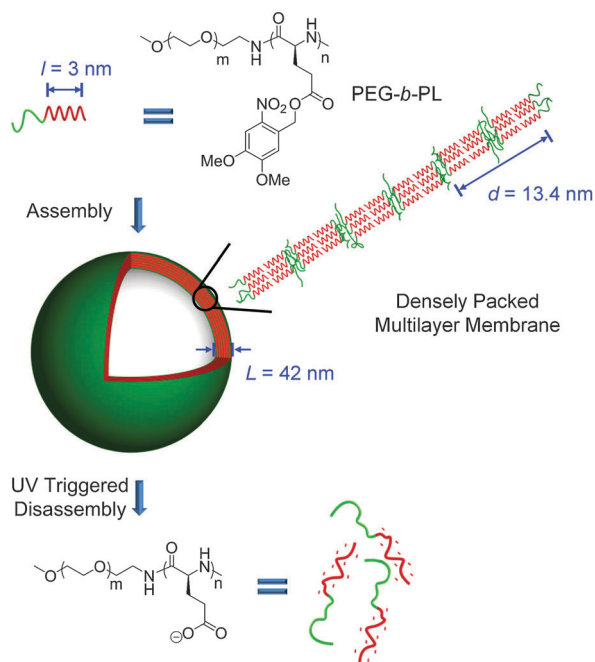
Fig. 1 Schematic illustration of polypeptide vesicle formation with densely packed multilayer membrane and UV-triggered disassembly process. The polypeptide length l is estimated by assuming ideal α-helical conformation, the layer thickness d and the membrane thickness (domain size) L are estimated from SAXS results.

structure.[25,26] Given the rigidity of polypeptide rods compared to lipids, polypeptide vesicles with such nanometer-thin stiff membrane may have compromised vesicle stability and poorly controlled membrane permeability.

In this article, we use poly(ethylene glycol)-*block*-poly(γ-(4,5-dimethoxy-2-nitrobenzyl)-L-glutamate) (PEG-*b*-PL), a rod-coil diblock polymeric amphiphile with a hydrophobic polypeptide segment, to show how the membrane structures of polypeptide vesicles can be manipulated. With cryogenic TEM and X-ray scattering techniques, we show for the first time clear evidence of densely packed multilayer membrane structures of polypeptide vesicles. These structures result presumably from further assembly of unstable unilamellar structures, and closely resemble liposomal multilamellar vesicle (MLV) membrane structures with the absence of water spacing between layers (Fig. 1). Random-coil PEG segments play an important role in segregating the PL macromolecular rods into a smectic-like ordering, while being short enough to be collapsed and buried between the layers of polypeptide helices. Although α-helical polypeptides such as poly(γ-benzyl-L-glutamate) (PBLG) often pack nematically with long-range directional order but no positional order,[27–30] we are able to obtain smectic ordering of rod-like polypeptides through the use of flexible PEG domains whereas previously this packing could only be obtained through the use of genetically engineered monodisperse polypeptides.[31,32] The incorporation of photo-responsive PL segments also enables the study of the triggered disassembly of such vesicles by changing the side-chain charge state and disrupting the amphiphilic structure (Fig. 1).

Experimental section

Materials

All chemicals were purchased from Sigma-Aldrich (St. Louis, MO, USA) and used as received unless otherwise specified. Anhydrous *N,N*-dimethylformamide (DMF) was dried by a column packed with 4 Å molecular sieves and stored in a glovebox. Anhydrous tetrahydrofuran (THF) and hexane were dried by a column packed with alumina. Methoxy poly(ethylene glycol) amines (mPEG-NH$_2$, 1 kDa, 2 kDa and 5 kDa) were purchased from Laysan Bio (Arab, AL, USA). Spectra/Por RC dialysis tubings with molecular weight cut off (MWCO) of 1 kDa were purchased from Spectrum Laboratories (Rancho Dominguez, CA, USA). Carbon film and holey carbon film supported copper grids (200 mesh) were purchased from Electron Microscopy Sciences (Hatfield, PA, USA).

Instrumentation

^{1}H nuclear magnetic resonance (NMR) spectra were recorded on a Varian U500 MHz or a VXR-500 MHz spectrometer. Chemical shifts were reported in ppm and referenced to the solvent proton impurities. Gel permeation chromatography (GPC) experiments were performed on a system equipped with an isocratic pump (Model 1100, Agilent Technology, Santa Clara, CA, USA), a DAWN HELEOS multi-angle laser light scattering (MALLS) detector (Wyatt Technology, Santa Barbara, CA, USA), and an Optilab rEX refractive index detector (Wyatt Technology, Santa Barbara, CA, USA). The detection wavelength of HELEOS was set at 658 nm. Separations were performed using serially connected size exclusion columns (10^2 Å, 10^3 Å, 10^4 Å, 10^5 Å, and 10^6 Å Phenogel columns, 5 μm, 300 × 7.8 mm, Phenomenex, Torrance, CA, USA) at 60 °C using DMF containing 0.1 mol L^{-1} LiBr as the mobile phase. The MALLS detector was calibrated using pure toluene and can be used for the determination of the absolute molecular weights. The MWs of polymers were determined based on the dn/dc value of each polymer sample calculated offline by using the internal calibration system processed by the ASTRA 6 software (version 6.1.1.17, Wyatt Technology, Santa Barbara, CA, USA). Circular dichroism (CD) measurements were carried out on a JASCO J-815 CD spectrometer (JASCO, Easton, MD, USA). The polymer samples were prepared at a concentration of 0.40 mg mL^{-1} in aqueous solution at pH = 7 and the solution was placed in a quartz cell with a pathlength of 0.10 cm. The mean residue molar ellipticity of each polypeptide was calculated on the basis of the measured apparent ellipticity by following the literature-reported formulas: ellipticity ($[\theta]$ in deg cm^2 dmol^{-1}) = (millidegrees × mean residue weight)/(path length in millimetres × concentration of polypeptide in mg mL^{-1}).[33,34] Transmission electron microscopy (TEM) and cryogenic TEM (cryo-TEM) images were collected using JEOL 2100 cryo transmission electron microscope. Ultra-violet (UV) light was generated from an OmniCure S1000 UV lamp (Lumen Dynamics Group, Mississauga, Ontario, Canada). Infrared spectra were recorded on a Perkin Elmer 100 serial FTIR spectrophotometer calibrated with polystyrene film (PerkinElmer, Santa Clara, CA, USA). Fluorescent spectra were recorded on a

Perkin Elmer LS 55 fluorescence spectrometer (PerkinElmer, Santa Clara, CA, USA).

Synthesis of γ-(4,5-dimethoxy-2-nitrobenzyl)-L-glutamate (DMNB-L-Glu) and γ-(4,5-dimethoxy-2-nitrobenzyl)-D-glutamate (DMNB-D-Glu)

DMNB-L-Glu was synthesized following the reported procedure.[19] In a 250 mL flat bottom flask, N,N,N',N'-tetramethylguanidine (1.1 mL, 8.77 mmol) was added dropwise to a stirred mixture of L-glutamic acid (0.65 g, 4.45 mmol) and L-glutamic acid copper(II) complex (1.05 g, 2.15 mmol) in DMF (4.0 mL) and distilled (DI) water (0.6 mL). The solution was stirred at room temperature for 2 h until all solids were dissolved and then more DMF (3.0 mL) was added. 4,5-Dimethoxy-2-nitrobenzyl bromide (2.5 g, 9.06 mmol) was added to the above solution in one portion. The reaction mixture was stirred at 40 °C for 24 h. Acetone (100 mL) was added to the mixture and stirred for 2 h until a fine precipitate was obtained. The violet solid was collected by filtration, followed by mixing with freshly prepared ethylenediaminetetraacetic acid (1.89 g)/sodium bicarbonate (1.08 g) aqueous solution (15 mL) to remove excessive copper salts. The mixture was stirred for another 24 h. The crude product was collected by filtration and washed with DI water. The solid was further purified by recrystallization from isopropanol/DI water (1 : 1, v/v). Isopropanol was then removed under vacuum and DI water was removed via lyophilization to yield the final product DMNB-L-Glu as light yellow powder (1.74 g, 77% yield). The glassware was wrapped with aluminum foil to avoid light exposure during the whole process. ^{1}H NMR (DMSO-d_6/D$_2$O–DCl (35 wt%), 9 : 1, v/v): δ 7.59 (s, 1H, ArH), 7.11 (s, 1H, ArH), 5.30 (s, 2H, ArCH_2–), 3.86 (t, 1H, α-H), 3.83 (s, 3H, CH_3O–), 3.78 (s, 3H, CH_3O–), 2.60 (m, 2H, –CH$_2$CH_2CO–), 2.04 (m, 2H, –CH_2CH$_2$CO–).

DMNB-D-Glu was synthesized similarly using D-glutamic acid and D-glutamic acid copper(II) complex. The final product was obtained as light yellow powder (78% yield). ^{1}H NMR (DMSO-d_6/D$_2$O–DCl (35 wt%), 9 : 1, v/v): δ 7.58 (s, 1H, ArH), 7.10 (s, 1H, ArH), 5.29 (s, 2H, ArCH_2–), 3.85 (t, 1H, α-H), 3.82 (s, 3H, CH_3O–), 3.77 (s, 3H, CH_3O–), 2.58 (m, 2H, –CH$_2$CH_2CO–), 2.03 (m, 2H, –COCH_2CH$_2$–).

Synthesis of γ-(4,5-dimethoxy-2-nitrobenzyl)-L-glutamate N-carboxyanhydride (DMNB-L-Glu-NCA) and γ-(4,5-dimethoxy-2-nitrobenzyl)-D-glutamate N-carboxyanhydride (DMNB-D-Glu-NCA)

In a dried 250 mL two-neck round bottom flask, DMNB-L-Glu (0.70 g, 2.04 mmol) was added and dried under vacuum for 2 h. Phosgene (15 wt% in toluene, 2.0 mL, 2.80 mmol) was added along with anhydrous THF (30 mL), the mixture was stirred at 50 °C for 2 h under the protection of drying tube. Solvent THF was then removed under vacuum to obtain a yellow solid. The crude product was purified by recrystallization from THF–hexane (1 : 5, v/v) three times in a glovebox to obtain light yellow crystal (0.63 g, 84% yield). The resulting DMNB-L-Glu-NCA monomer was stored at −30 °C in the glovebox. The glassware was wrapped with aluminum foil to avoid light exposure during the whole process. ^{1}H NMR (CDCl$_3$): δ 7.70 (s, 1H, ArH), 6.97

(s, 1H, ArH), 6.50 (s, 1H, NH), 5.48 (q, 2H, ArCH_2–), 4.46 (t, 1H, α-H), 4.00 (s, 3H, CH_3O–), 3.96 (s, 3H, CH_3O–), 2.65 (t, 2H, –CH$_2$CH_2CO–), 2.24 (m, 2H, –CH_2CH$_2$CO–). ^{13}C NMR (CDCl$_3$): δ 172.2, 169.6, 153.7, 151.9, 148.9, 140.5, 125.9, 111.6, 108.6, 64.4, 57.0, 56.8, 56.7, 29.8, 27.1.

DMNB-D-Glu-NCA was synthesized similarly using DMNB-D-Glu. The final product was obtained as light yellow crystal (80% yield). ^{1}H NMR (CDCl$_3$): δ 7.71 (s, 1H, ArH), 6.97 (s, 1H, ArH), 6.20 (s, 1H, NH), 5.50 (q, 2H, ArCH_2–), 4.44 (t, 1H, α-H), 4.01 (s, 3H, CH_3O–), 3.97 (s, 3H, CH_3O–), 2.65 (t, 2H, –CH$_2$CH_2CO–), 2.26 (m, 2H, –CH_2CH$_2$CO–).

Synthesis of poly(ethylene glycol)-block-poly(γ-(4,5-dimethoxy-2-nitrobenzyl)-L-glutamate) (PEG-b-PL), poly(ethylene glycol)-block-poly(γ-(4,5-dimethoxy-2-nitrobenzyl)-D-glutamate) (PEG-b-PD) and poly(ethylene glycol)-block-poly(γ-(4,5-dimethoxy-2-nitrobenzyl)-DL-glutamate) (PEG-b-PDL)

In a glovebox, DMNB-L-Glu-NCA (60 mg, 0.16 mmol) was dissolved in DMF (1.50 mL), followed by adding the DMF solution of mPEG-NH$_2$ (0.02 mol L^{-1}, 407 µL, 0.008 mmol, M/I = 20). The polymerization mixture was stirred at room temperature. FTIR was used to monitor the polymerization until the conversion was above 99%. The polymer was then precipitated by cold hexane/ether (1 : 1, v/v) and collected by centrifugation. The final polymer PEG-b-PL was obtained as viscous yellow solid after removing the solvent residue under vacuum (80–87% yield). The glassware was wrapped with aluminum foil to avoid light exposure during the whole process. ^{1}H NMR (CDCl$_3$/TFA-d, 85 : 15, v/v): δ 7.66 (s, 1H, ArH), 6.97 (s, 1H, ArH), 5.40 (s, 2H, ArCH_2–), 4.67 (s, 1H, α-H), 3.94 (s, 3H, CH_3O–), 3.92 (s, 3H, CH_3O–), 3.78 (s, 4H, –OCH_2CH_2–), 2.59 (s, 2H, –COCH_2CH$_2$–), 2.14 (d, 2H, –COCH$_2$CH_2–).

PEG-b-PD was synthesized similarly using DMNB-D-Glu-NCA as the monomer. The final product was obtained as a viscous yellow solid (82–85% yield). ^{1}H NMR (CDCl$_3$/TFA-d, 85 : 15, v/v): δ 7.65 (s, 1H, ArH), 6.96 (s, 1H, ArH), 5.39 (s, 2H, ArCH_2–), 4.64 (s, 1H, α-H), 3.93 (s, 3H, CH_3O–), 3.92 (s, 3H, CH_3O–), 3.77 (s, 4H, –OCH_2CH_2–), 2.59 (s, 2H, –COCH_2CH$_2$–), 2.13 (d, 2H, –COCH$_2$CH_2–).

PEG-b-PDL was synthesized similarly by mixing DMNB-L-Glu-NCA and DMNB-D-Glu-NCA with a 1 : 1 ratio as the monomers. The final product was obtained as yellow solid (78–82% yield). ^{1}H NMR (CDCl$_3$/TFA-d, 85 : 15, v/v): δ 7.63 (s, 1H, ArH), 6.97 (s, 1H, ArH), 5.38 (s, 2H, ArCH_2–), 4.64 (s, 1H, α-H), 3.93 (s, 6H, CH_3O–), 3.76 (s, 4H, –OCH_2CH_2–), 2.58 (s, 2H, –COCH_2CH$_2$–), 2.14 (d, 2H, –COCH$_2$CH_2–).

Preparation of copolymer self-assemblies in aqueous solution

Dried PEG-b-PL diblock copolymer powder (5 mg, or with 0.1 wt% Nile Red) was dissolved in DMF (1.0 mL) in a small vial charged with a magnetic stir bar, followed by dropwise addition of DI water (4.0 mL) via syringe pump (KD Scientific, Holliston, MA, USA. Addition speed: 0.1 mL min^{-1}). The suspension was stirred at room temperature for 2 h, and then transferred to a dialysis bag (MWCO = 1 kDa). The assemblies were dialyzed against DI water for 4 h to remove DMF (water changed

every hour). The resulting suspension was used for subsequent studies.

Transmission electron microscopy (TEM)

TEM samples were prepared on carbon film supported copper grids (200 mesh). One drop (~ 10 μL) of diluted copolymer assembly aqueous suspension (0.25–0.5 mg mL^{-1}) was placed on the grid and allowed to interact with the surface for 10 min. Filter paper was then used to remove the residual polymers and liquid. The sample on the grid was imaged using JEOL 2100 cryo TEM at 80 kV.

Cryogenic transmission electron microscopy (Cryo-TEM)

Cryo-TEM samples were prepared on holey carbon film supported copper grids (200 mesh) using Vitrobot (FEI, Hillsboro, OR, USA). One drop (~ 10 μL) of diluted copolymer assembly aqueous suspension (0.25–0.5 mg mL^{-1}) was placed on the grid, and the drop was blotted with blotting paper. The solution residue was then vitrified by rapidly immersing it into liquid ethane. The vitrified sample was transferred to a JEOL 2100 cryo TEM microscope for imaging using a cryo-holder at 200 kV. The temperature of the sample was kept below -180 °C during the course of sample preparation and imaging.

Small/wide-angle X-ray scattering (SAXS/WAXS)

Copolymer assembly samples were prepared in 1.5 mm quartz X-ray capillaries (Hilgenberg Glas, Germany) and the SAXS/WAXS experiments were conducted in a home built (Forvis Technologies, Santa Barbara, CA, USA) equipment composed of a Xenocs GeniX3D CuKα Ultra Low Divergence X-ray source (1.54 Å/8 keV), with a divergence of ~ 1.3 mrad. The 2D diffraction data were radially averaged upon acquisition on a Pilatus 300 K 20 Hz hybrid pixel Detector (Dectris) and integrated using FIT2D software (http://www.esrf.eu/computing/scientific/FIT2D) from ESRF.[35,36]

UV irradiation studies

The copolymer aqueous suspension (1.0 mL) was transferred to a small vial charged with a magnetic stir bar, the vial was then placed under UV lamp for UV irradiation ($\lambda = 365$ nm, $I = 0$–50 mW cm^{-2}, $t = 0$–30 min). The UV intensity and irradiation time was controlled through the UV lamp to study the disassembly process.

Results and discussion

We prepared PEG-polypeptide amphiphilic diblock copolymers through ring-opening polymerization (ROP) of γ-(4,5-dimethoxy-2-nitrobenzyl)-L-glutamate N-carboxyanhydride (DMNB-L-Glu-NCA) (Scheme S1 and Fig. S1–S5†).[19] The resulting diblock copolymers are named as PEG$_m$-b-PX$_n$, where "m" is the MW of PEG, "n" is the degree of polymerization (DP) of polypeptides, and "X" refers to the stereochemistry of the amino acid residues of the polypeptide block (L, D or DL). Since previously reported polypeptide vesicles only have ~ 20 hydrophobic polypeptide repeating units in

their bilayer structure,[25,26,37–41] we first evaluated whether high MW polypeptides could be used to prepare vesicles with thick membranes and, thus, potentially improved stability. We synthesized PEG$_{1k}$-b-PL$_{100}$ and used the co-solvent method[42] to drive the formation of self-assembled structures. After water was dropwise added into the DMF solution of PEG$_{1k}$-b-PL$_{100}$, macroscopic precipitation was observed instead of self-assembly, suggesting uncontrolled polypeptide chain interaction. The relatively short hydrophilic PEG block may not be able to prevent the random packing of rod-like polypeptides.[25]

Copolymers with reduced polypeptide DP were then synthesized in order to better control helix–helix packing for stable colloidal suspensions. Self-assemblies from three amphiphilic copolymers with shorter polypeptide lengths, PEG$_{1k}$-b-PL$_{10}$, PEG$_{1k}$-b-PL$_{20}$, and PEG$_{1k}$-b-PL$_{40}$, were prepared. The α-helical conformation of the synthesized PL blocks in aqueous environment was confirmed by circular dichroism (CD) and ATR-FTIR spectroscopy (Fig. S6 and S7†). Based on the TEM analysis, we found that PEG$_{1k}$-b-PL$_{20}$ could largely form hollow vesicular structures with a diameter around 400 nm through closure of the lamellar membrane (Fig. 2B). Such PEG/polypeptide ratio was found to be crucial to form stable vesicular morphology. PEG$_{1k}$-b-PL$_{10}$ copolymers showed irregular membrane structures presumably because of the weak interaction of the ultra-short polypeptide (PL 10-mer) (Fig. 2A).[26] PEG$_{1k}$-b-PL$_{40}$ mainly formed large broken pieces of membrane likely due to the stiff nature of the PL 40-mer, which makes it difficult for the membrane to curve into vesicles (Fig. 2C).[25] In addition, we noticed all three copolymer assemblies showed uncommonly high contrast on carbon film grids without staining. This observation was quite different from other amphiphiles with similar lengths (e.g., lipids), indicating a thick membrane structure (Fig. S8†).

In order to understand how copolymer composition and polypeptide conformation influence the assembly structure,[25,26,38] we synthesized four more polypeptides with variable PEG lengths and polypeptide conformations. PEG$_{2k}$-b-PL$_{20}$ and PEG$_{2k}$-b-PL$_{40}$, with increased hydrophilic PEG size and bulkiness, showed the sheet-like typical bilayer membrane structures with low contrast in the absence of stain (Fig. 2D, E and Fig. S8†). The self-assembly of PEG$_{1k}$-b-PD$_{20}$ and PEG$_{1k}$-b-PDL$_{20}$ were also studied to elucidate the effects of polypeptide conformation on the self-assembled structures. CD analysis indicated PD segments adopted left-handed α-helical conformation, while the racemic PDL block showed a random-coil conformation with no Cotton effect (Fig. S6†). PEG$_{1k}$-b-PD$_{20}$ assemblies exhibited similar hollow vesicular morphology with thick membranes, substantiating that the helical sense has no effect on the assembly behavior (Fig. 2F). Racemic PEG$_{1k}$-b-PDL$_{20}$ only formed large compound micelles instead of 2D sheets (Fig. 2G),[42,43] similar as what was previously reported for polypeptide vesicles with random-coil hydrophobic polypeptide blocks.[25,26] In the absence of side-by-side ordering of helical polypeptide rods, coil–coil diblock copolymers with pure hydrophobic effects cannot form stable bilayer membrane at relatively low hydrophobic-to-hydrophilic ratio.[2,25,26,39]

From the self-assembly behavior of the seven copolymers shown in Table 1, we have clearly shown that both morphology
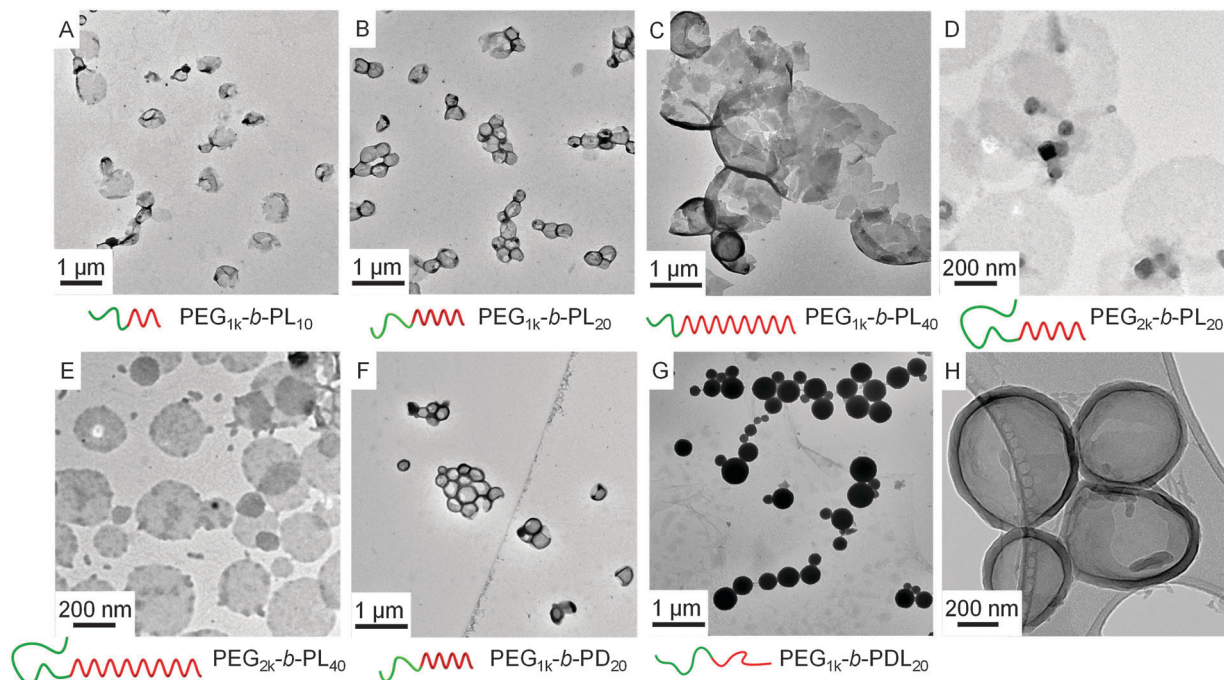
Fig. 2 The self-assembly morphology of amphiphilic diblock copolymers PEG-*b*-polypeptide. (A–E) Composition-dependent self-assembly morphology: (A) PEG_{1k}-*b*-PL_{10}, (B) PEG_{1k}-*b*-PL_{20}, (C) PEG_{1k}-*b*-PL_{40}, (D) PEG_{2k}-*b*-PL_{20} and (E) PEG_{2k}-*b*-PL_{40}. (F and G) Conformation-dependent self-assembly morphology: (F) PEG_{1k}-*b*-PD_{20} and (G) PEG_{1k}-*b*-PDL_{20}. (H) Cryogenic TEM images of PEG_{1k}-*b*-PL_{20} vesicle.

and membrane structures of PEG-*b*-PL assemblies are governed not only by the block composition of amphiphiles but also the conformation of hydrophobic segments. The membrane structures of assemblies were also studied by cryogenic TEM (cryo-TEM) to confirm the difference between PEG_{1k}-*b*-PL and PEG_{2k}-*b*-PL assemblies. PEG_{1k}-*b*-PL_{20} showed uniform, hollow vesicular structures with high contrast (Fig. 2H and Fig. S9†). The membrane thickness was estimated to be 40 nm, which is much thicker than typical bilayer structure ($\sim$6 nm for two polypeptide blocks with DP = 20, assuming ideal α-helix). On the other hand, PEG_{2k}-*b*-PL_{40} showed spherical sheets with much lower contrast (Fig. S9†).

We propose that the formation of the unusually thick membrane of PEG_{1k}-*b*-PL is due to the further assembly of "unstable" bilayer sheets into a multilayer structure (Fig. 3).

Two interactions may play a role in the assembly of these multilayer structures. First, previous work on polypeptide based rod-coil amphiphiles demonstrates that the interactions between α-helical rigid rod-like hydrophobic segments first drive the formation of 2D bilayer sheets through anisotropic side-by-side ordering.[25,26] Since conformational entropy loss during the segregation process of stiff helical polypeptides is insignificant, the minimization of interfacial energy dominates the assembly process of PEG-*b*-PL forming bilayer structures.[2] Second, the interaction between the formed bilayer and the solvent is relatively high in energy, as the PEG is not long and bulky enough to fully solvate and stabilize the formed bilayer in the aqueous environment. This leads to higher interfacial energy at
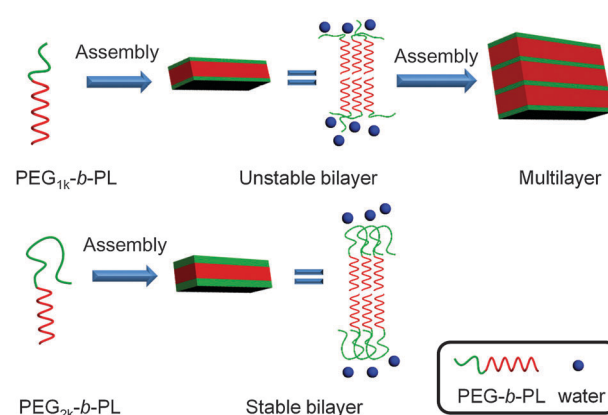
Table 1 The compositions of the PEG-*b*-polypeptide copolymers and their self-assembled structures

Copolymer	Composition[a]	Morphology[b]	Membrane[c]
PEG_{1k}-*b*-PL_{10}	PEG_{22}-*b*-PL_{10}	V, I	Multilayer
PEG_{1k}-*b*-PL_{20}	PEG_{22}-*b*-PL_{22}	V	Multilayer
PEG_{1k}-*b*-PL_{40}	PEG_{22}-*b*-PL_{44}	I	Multilayer
PEG_{2k}-*b*-PL_{20}	PEG_{44}-*b*-PL_{20}	S	Bilayer
PEG_{2k}-*b*-PL_{40}	PEG_{44}-*b*-PL_{38}	S	Bilayer
PEG_{1k}-*b*-PD_{20}	PEG_{22}-*b*-PD_{22}	V	Multilayer
PEG_{1k}-*b*-PDL_{20}	PEG_{22}-*b*-PDL_{22}	LCM	—

[a] Obtained copolymer composition determined by ^{1}H NMR. [b] Morphology determined visually from regular TEM images. V = vesicles; I = irregular aggregates, S = membrane sheets, LCM = large compound micelle. [c] Membrane structure determined by cryo-TEM images and SAXS results.

Fig. 3 Proposed self-assembly process of PEG_{1k}-*b*-PL to form multilayer membrane and PEG_{2k}-*b*-PL to form bilayer membrane.

the hydrophobic–hydrophilic interface, resulting in unstable bilayers subject to further assembly for minimized interfacial energy. The bilayers assemble and form multilayer structures with PEG segments collapsed and buried between polypeptide helical domains and water molecules excluded between bilayers (Fig. 3). To our best knowledge, this is the first report of further assembly of unstable bilayers into densely packed multilayer membrane structures in polymersomes.

The use of PEG_{1k} as the hydrophilic block is important in this polypeptide-based assembly system. PEG_{1k} block is not only an effective separator to segregate the polypeptides, but also acts as a short and flexible unit connecting the helical layers. PEG_{2k}, when used in the amphiphilic copolymer, provides sufficient solubilizing ability and bulkiness to hydrate and stabilize the bilayer membrane in aqueous solution, which prefers to form traditional bilayer membrane with low interfacial energy (Fig. 3). The increased size and hydrophilicity of PEG_{2k} segments also make it difficult to be buried between layers of helices; therefore, PEG_{2k}-b-PL assembled membranes resemble the previous reported polypeptide vesicle systems,[25,26,37–40] which used sterically hindered hydrophilic polymer blocks including oligo(ethylene glycol) based α-helical polypeptides,[25] glycopolypeptides,[38,40] Y-shaped branched PEG,[39] or charged polypeptides that prevented close-packing of bilayers.[26,37] Similar as PEG_{2k}-b-PL, the further assembly of bilayers in these systems is therefore not favored considering the bulkiness or the charge repulsion of these hydrophilic segments.

To confirm the multilayered structures and further elucidate how PEG_{1k}-b-PL amphiphiles were arranged in the membrane, small-angle X-ray scattering (SAXS) and wide-angle X-ray scattering (WAXS) were used to analyze five assemblies in aqueous suspensions (Fig. 4A and B). In the SAXS regime, a Bragg peak was observed for the PEG_{1k}-b-PL assembly at the characteristic distances of $d = 2\pi/q$ (nm): PEG_{1k}-b-PL_{10} ($d = 12.2$), PEG_{1k}-b-PL_{20} ($d = 13.4$), and PEG_{1k}-b-PL_{40} ($d = 18.5$). A weak second order Bragg peak was also observed for the PEG_{1k}-b-PL_{40} sample (at $d = 9.0$ nm) (Fig. 4A). These results indicate the existence of a multilayer arrangement in all PEG_{1k}-b-PL membranes, where each layer comprises about 8, 4, and 3 copolymer units of PEG_{1k}-b-PL_{10}, PEG_{1k}-b-PL_{20}, and PEG_{1k}-b-PL_{40}, respectively (assuming ideal α-helix, 0.15 nm per polypeptide repeating unit). The membrane thickness of self-assemblies, or in other words, the domain size L which relates to the number of layers in each membrane estimated by the full width at half maximum of the primary Bragg peaks, is determined to be $L = 32$, 42, 49 nm for PEG_{1k}-b-PL_{10}, PEG_{1k}-b-PL_{20}, and PEG_{1k}-b-PL_{40}, respectively (Fig. 1). The results correlate well with the membrane thickness observed by cryo-TEM of PEG_{1k}-b-PL_{20} (40 nm). One should note that the Bragg reflections in the SAXS regime are rather broad. While there are many possible reasons for peak broadening, we should expect to obtain a local distribution of d spacings for PEG-b-PL assemblies due to the fact that the PEG moiety is flexible and may act as a 'spring' between hydrophobic PL units. In addition, the fact that there is no water within the multilayers affects the contrast of the X-ray signal. While the PEG domains make the peaks broader, it
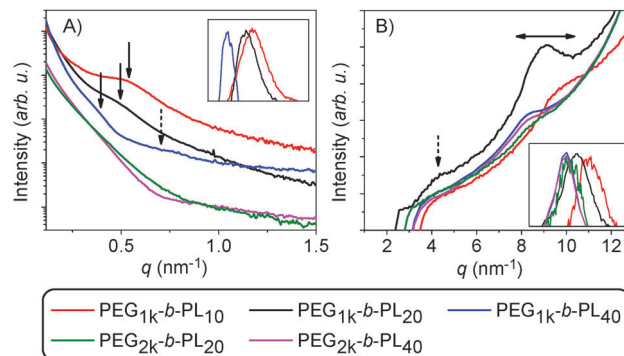

Fig. 4 X-ray scattering scans obtained for five different assemblies of PEG-b-PL. (A) SAXS scans (log$y$) reveal a Bragg reflection (indicated by solid arrow) at the characteristic repeat distances of $d = 2\pi/q$ = 12.2, 13.4 and 18.5 nm for PEG_{1k}-b-PL_{10}, PEG_{1k}-b-PL_{20}, and PEG_{1k}-b-PL_{40}, respectively. A weak second order Bragg peak (indicated by the dash arrow) is also observed for the PEG_{1k}-b-PL_{40} sample (at repeat distance $d = 9.0$ nm). The peak positions were determined by a Gaussian fit to the SAXS lines after a polynomial background reduction. The subtracted SAXS data in the q interval of the first peak is shown on the inset. (B) WAXS scans show a prominent Bragg peak (indicated by solid arrow) at characteristic distance d (nm) observed for all assemblies. PEG_{1k}-b-PL_{10} ($d = 0.66$), PEG_{1k}-b-PL_{20} ($d = 0.71$), PEG_{1k}-b-PL_{40} ($d = 0.77$), PEG_{2k}-b-PL_{20} ($d = 0.75$), and PEG_{2k}-b-PL_{40} ($d = 0.77$). Another weak Bragg peak (indicated by the dash arrow) is also observed for PEG_{1k}-b-PL_{20} suspension (at repeat distance $d = 1.4$ nm). The peak positions were determined by a Gaussian fit to the WAXS lines after a polynomial background reduction shown on the inset.

is also their size, relative to the polypeptide segment, affects the degree of ordering. For example, the PEG_{1k}-b-PL_{10} membrane gives rise to the strongest Bragg peak intensity compared to other copolymers, indicating a more ordered smectic phase. The hydrophilic PEG domain is an effective separator to segregate the PL block, and also function as a 'spring' to compensate the geometrical mismatch of polypeptide layer. Increase of the polypeptide length, with reduced fraction of PEG_{1k}, results in decreased segregation effects between helical domains and decreased geometrical compensation effects, eventually leading to uncontrolled packing (as PEG_{1k}-b-PL_{100} mentioned above). Indeed, for the PEG_{2k}-b-PL systems where the membrane can barely be observed or appears to be very thin in TEM, no Bragg reflections were detected by SAXS.

Fig. 4B shows the WAXS data obtained for all assemblies. A prominent reflection at the characteristic spacings of $d = 2\pi/q$ (nm) is observed for all the samples: PEG_{1k}-b-PL_{10} ($d = 0.66$), PEG_{1k}-b-PL_{20} ($d = 0.71$), PEG_{1k}-b-PL_{40} ($d = 0.77$), PEG_{2k}-b-PL_{20} ($d = 0.75$), and PEG_{2k}-b-PL_{40} ($d = 0.77$). Regardless of segment length, these Bragg reflections result from the rise per turn as previously reported.[44] In addition, we also observed another low intensity Bragg peak at low q ($q = 4.5$ nm^{-1}) before the most prominent peak at $ca.$ $q = 9$ nm^{-1} for PEG_{1k}-b-PL_{20}. The corresponding distance 1.4 nm matches the diameter of α-helical polypeptides.[45] This WAXS reflection arises from a lateral short range order of the polypeptides within the bilayer membrane as similarly observed in other α-helix systems.[31] Through Gaussian peak fitting, the short range order domain size of PEG_{1k}-b-PL_{20} vesicles in lateral direction is calculated as approximately 2.4 nm,
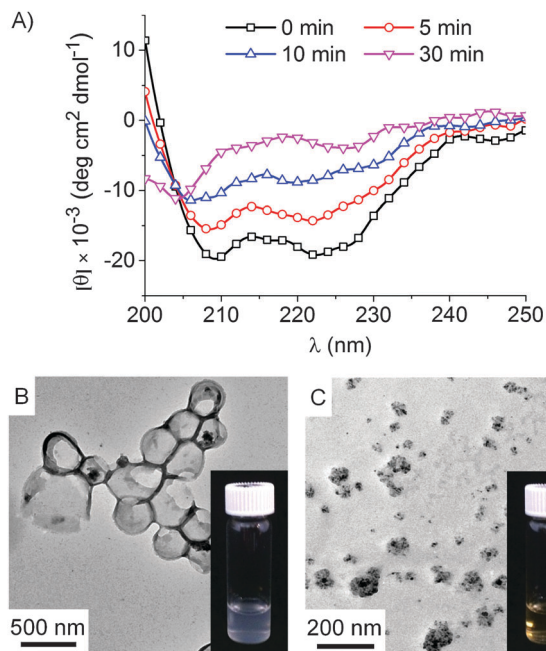
Fig. 5 Disassembly of polypeptide vesicles upon UV irradiation (λ = 365 nm). (A) CD spectra of PEG_{5k}-b-PL_{20} upon UV irradiation at 10 mW cm^{-2} for 0, 5, 10 and 30 min. PEG_{5k} was used to solubilize PL segments in aqueous solution for CD tests; (B, C) TEM images of PEG_{1k}-b-PL_{20} before and after UV irradiation (10 min, 10 mW cm^{-2}). The insets show photography of PEG_{1k}-b-PL_{20} aqueous suspension before and after UV irradiation.

which corresponds to about two units. With more understandings on copolymer arrangement in the multilayer membranes from the X-ray scattering studies, it is clear that the multilayer membrane from PEG-b-PL assembly is structurally different from the liposomal MLV and other multilamellar polymersome as no water is found in the densely packed multilayer membrane structure (Fig. 1).[7,46,47]

When stimuli responsive functionalities are introduced in vesicle-forming polymeric amphiphiles, it is possible to control the morphological transition or membrane permeability, thus potentially broaden the application of polymersomes in encapsulation and delivery.[10,11,14,22] As the copolymer has built-in photo-responsive PL domain, we next studied the trigger-induced disassembly of PEG_{1k}-b-PL_{20} vesicles. Under UV irradiation, the cleavage of the 4,5-dimethoxy-2-nitrobenzyl (DMNB) ester bond results in the transition from the hydrophobic, α-helical PL to the anionic, random-coil poly(L-glutamic acid) (Fig. 1). The elimination of the PL helical structure was verified by CD spectroscopy (Fig. 5A). This conformation change, together with the change of amphiphilicity of the copolymer, induced the disassembly of vesicles. After 10 min UV irradiation, the turbid vesicle suspension became yellowish and clear, indicating the release of the DMNB group and the complete disassembly of the self-assembled structure. The resulting post-irradiation samples were further analyzed by TEM, which showed the disappearance of regular hollow spherical structures previously observed and the formation of irregular aggregates from PEG-b-poly(glutamic acid) dried on the TEM grid (Fig. 5B and C). All other self-assemblies from

PEG-b-PL diblock copolymers exhibited similar turbidity and color change, indicating the same disassembly mechanism as PEG_{1k}-b-PL_{20} vesicles. Nile Red was used as a hydrophobic indicator to evaluate the UV-responsiveness of PEG_{1k}-b-PL_{20} vesicles.[48] The disassembly process was studied with different UV intensities and irradiation times, taking advantage of the tunability and precise control of the light trigger.[49–51] By changing the UV intensity from 0.5 to 50 mW cm^{-2}, we were able to successfully control the disassembly kinetics. Lower UV intensity led to a slower disassembly process, while longer irradiation time (10 min) completely disrupted the vesicle structure (Fig. S10†).

Conclusions

We reported the formation of the unprecedented, densely packed multilayer membranes using PEG_{1k}-b-PL block copolymers. In such membrane, polypeptide rods exhibit smectic ordering, with PEG_{1k} segments buried between the layers of helices. The PEG_{1k} moiety behaves as an effective separator to enable polypeptide segregation, and is short enough to allow the interaction of the neighboring polypeptide layers for further assembly to eventually form the multilayered structures. Tuning copolymer composition and polypeptide conformation lead to the change of self-assembly morphology and membrane structures. When diblock copolymer composition is properly adjusted (PEG_{1k}-b-PL_{20}), a hollow vesicular morphology is obtained. UV irradiation alters polypeptide conformation and copolymer amphiphilicity, resulting in the complete disassembly of self-assembled structures. The combination of thick membrane structures and trigger-responsive moieties in this new polypeptide vesicle may open up new opportunities for the design of membranes of encapsulation and delivery systems with improved barrier properties. Meanwhile, the unique vesicle membrane structures may also provide new insights into the self-assembly behavior of rod-coil block copolymers, showing how precise control of block copolymer composition and secondary structure influence the molecular arrangement and eventually control the morphology and membrane structures of assemblies.

Acknowledgements

References

1 D. E. Discher and A. Eisenberg, *Science*, 2002, **297**, 967–973.
2 M. Antonietti and S. Forster, *Adv. Mater.*, 2003, **15**, 1323–1333.
3 D. E. Discher, V. Ortiz, G. Srinivas, M. L. Klein, Y. Kim, C. A. David, S. S. Cai, P. Photos and F. Ahmed, *Prog. Polym. Sci.*, 2007, **32**, 838–857.

4 D. H. Levine, P. P. Ghoroghchian, J. Freudenberg, G. Zhang, M. J. Therien, M. I. Greene, D. A. Hammer and R. Murali, *Methods*, 2008, **46**, 25–32.

5 D. A. Christian, S. Cai, D. M. Bowen, Y. Kim, J. D. Pajerowski and D. E. Discher, *Eur. J. Pharm. Biopharm.*, 2009, **71**, 463–474.

6 J. S. Lee and J. Feijen, *J. Controlled Release*, 2012, **161**, 473–483.

7 S. Rangelov and A. Pispas, *Polymer and Polymer-Hybrid Nanoparticles: From Synthesis to Biomedical Applications*, CRC Press, Boca Raton, FL, 2013.

8 B. M. Discher, Y.-Y. Won, D. S. Ege, J. C.-M. Lee, F. S. Bates, D. E. Discher and D. A. Hammer, *Science*, 1999, **284**, 1143–1146.

9 J. F. Le Meins, O. Sandre and S. Lecommandoux, *Eur. Phys. J. E: Soft Matter Biol. Phys.*, 2011, **34**, 1–17.

10 M.-H. Li and P. Keller, *Soft Matter*, 2009, **5**, 927–937.

11 F. Meng, Z. Zhong and J. Feijen, *Biomacromolecules*, 2009, **10**, 197–209.

12 H. A. Klok and S. Lecommandoux, *Adv. Mater.*, 2001, **13**, 1217–1229.

13 Y.-b. Lim, K.-S. Moon and M. Lee, *J. Mater. Chem.*, 2008, **18**, 2909–2918.

14 J. Zhang, X.-F. Chen, H.-B. Wei and X.-H. Wan, *Chem. Soc. Rev.*, 2013, **42**, 9127–9154.

15 H. Lu, J. Wang, Y. Bai, J. W. Lang, S. Liu, Y. Lin and J. Cheng, *Nat. Commun.*, 2011, **2**, 206.

16 N. P. Gabrielson, H. Lu, L. Yin, D. Li, F. Wang and J. Cheng, *Angew. Chem., Int. Ed.*, 2012, **51**, 1143–1147.

17 L. Yin, Z. Song, K. H. Kim, N. Zheng, N. P. Gabrielson and J. Cheng, *Adv. Mater.*, 2013, **25**, 3063–3070.

18 L. Yin, Z. Song, Q. Qu, K. H. Kim, N. Zheng, C. Yao, I. Chaudhury, H. Tang, N. P. Gabrielson, F. M. Uckun and J. Cheng, *Angew. Chem., Int. Ed.*, 2013, **52**, 5757–5761.

19 L. Yin, H. Tang, K. H. Kim, N. Zheng, Z. Song, N. P. Gabrielson, H. Lu and J. Cheng, *Angew. Chem., Int. Ed.*, 2013, **52**, 9182–9186.

20 H. Tang, L. Yin, K. H. Kim and J. Cheng, *Chem. Sci.*, 2013, **4**, 3839–3844.

21 Z. Song, N. Zheng, X. Ba, L. Yin, R. Zhang, L. Ma and J. Cheng, *Biomacromolecules*, 2014, **15**, 1491–1497.

22 A. Carlsen and S. Lecommandoux, *Curr. Opin. Colloid Interface Sci.*, 2009, **14**, 329–339.

23 C. Deng, J. Wu, R. Cheng, F. Meng, H.-A. Klok and Z. Zhong, *Prog. Polym. Sci.*, 2014, **39**, 330–364.

24 H. Lu, J. Wang, Z. Song, L. Yin, Y. Zhang, H. Tang, C. Tu, Y. Lin and J. Cheng, *Chem. Commun.*, 2014, **50**, 139–155.

25 E. G. Bellomo, M. D. Wyrsta, L. Pakstis, D. J. Pochan and T. J. Deming, *Nat. Mater.*, 2004, **3**, 244–248.

26 E. P. Holowka, D. J. Pochan and T. J. Deming, *J. Am. Chem. Soc.*, 2005, **127**, 12423–12428.

27 C. Robinson and J. C. Ward, *Nature*, 1957, **180**, 1183–1184.

28 C. Robinson, *Tetrahedron*, 1961, **13**, 219–234.

29 W. G. Miller and E. L. Wee, *J. Phys. Chem.*, 1971, **75**, 1446–1452.

30 J. C. Horton, A. M. Donald and A. Hill, *Nature*, 1990, **346**, 44–45.

31 S. M. Yu, V. P. Conticello, G. Zhang, C. Kayser, M. J. Fournier, T. L. Mason and D. A. Tirrell, *Nature*, 1997, **389**, 167–170.

32 S. M. Yu, C. M. Soto and D. A. Tirrell, *J. Am. Chem. Soc.*, 2000, **122**, 6552–6559.

33 A. J. Adler, N. J. Greenfield and G. D. Fasman, in *Methods Enzymol.*, ed. S. N. T. C. H. W. Hirs, Academic Press, 1973, vol. 27, pp. 675–735.

34 N. J. Greenfield, *Nat. Protoc.*, 2006, **1**, 2876–2890.

35 A. P. Hammersley, S. O. Svensson, M. Hanfland, A. N. Fitch and D. Hausermann, *High Pressure Res.*, 1996, **14**, 235–248.

36 A. P. Hammersley, ESRF Internal Report, 1998, ESRF98-HA01T, FIT2D V9.129 Reference Manual V123.121.

37 J. Rodriguez-Hernandez and S. Lecommandoux, *J. Am. Chem. Soc.*, 2005, **127**, 2026–2027.

38 J. Huang, C. Bonduelle, J. Thevenot, S. Lecommandoux and A. Heise, *J. Am. Chem. Soc.*, 2012, **134**, 119–122.

39 K. Osada, H. Cabral, Y. Mochida, S. Lee, K. Nagata, T. Matsuura, M. Yamamoto, Y. Anraku, A. Kishimura, N. Nishiyama and K. Kataoka, *J. Am. Chem. Soc.*, 2012, **134**, 13172–13175.

40 J. R. Kramer, A. R. Rodriguez, U.-J. Choe, D. T. Kamei and T. J. Deming, *Soft Matter*, 2013, **9**, 3389–3395.

41 A. R. Rodriguez, J. R. Kramer and T. J. Deming, *Biomacromolecules*, 2013, **14**, 3610–3614.

42 L. Zhang and A. Eisenberg, *Science*, 1995, **268**, 1728–1731.

43 Y. Mai and A. Eisenberg, *Chem. Soc. Rev.*, 2012, **41**, 5969–5985.

44 Y. Wang, F. L. Filho, P. Geil and G. W. Padua, *Macromol. Biosci.*, 2005, **5**, 1200–1208.

45 A. Niehoff, A. Mantion, R. McAloney, A. Huber, J. Falkenhagen, C. Goh, A. Thünemann, M. Winnik and H. Menzel, *Colloid Polym. Sci.*, 2013, **291**, 1353–1363.

46 A. Jesorka and O. Orwar, *Annu. Rev. Anal. Chem.*, 2008, **1**, 801–832.

47 A. Napoli, M. Valentini, N. Tirelli, M. Muller and J. A. Hubbell, *Nat. Mater.*, 2004, **3**, 183–189.

48 A. P. Goodwin, J. L. Mynar, Y. Ma, G. R. Fleming and J. M. J. Fréchet, *J. Am. Chem. Soc.*, 2005, **127**, 9952–9953.

49 N. Fomina, J. Sankaranarayanan and A. Almutairi, *Adv. Drug Delivery Rev.*, 2012, **64**, 1005–1020.

50 G. Liu and C.-M. Dong, *Biomacromolecules*, 2012, **13**, 1573–1583.

51 Y. Zhao, *Macromolecules*, 2012, **45**, 3647–3657.